Geophysical Research Letters

RESEARCH LETTER
10.1029/2022GL100961

Density Staircases Generated by Symmetric Instability in a Cross-Equatorial Deep Western Boundary Current

F. W. Goldsworth[1,2], H. L. Johnson[3], and D. P. Marshall[1]

[1]AOPP, Department of Physics, University of Oxford, Oxford, UK, [2]Oxford NERC Environmental Research DTP, Oxford, UK, [3]Department of Earth Sciences, University of Oxford, Oxford, UK

Key Points:

- Density staircases are observed in a high-resolution numerical model of a deep western boundary current crossing the equator
- As the deep western boundary current crosses the equator it becomes symmetrically unstable, generating overturning cells
- The overturning cells result in differential diapycnal mixing with well mixed regions separated by strongly stratified mixing barriers

Supporting Information:

Supporting Information may be found in the online version of this article.

Correspondence to:

F. W. Goldsworth,
frasergocean@gmail.com

Citation:

Goldsworth, F. W., Johnson, H. L., & Marshall, D. P. (2022). Density staircases generated by symmetric instability in a cross-equatorial deep western boundary current. *Geophysical Research Letters*, *49*, e2022GL100961. https://doi.org/10.1029/2022GL100961

Received 24 AUG 2022
Accepted 10 NOV 2022

Author Contributions:

Conceptualization: F. W. Goldsworth, H. L. Johnson, D. P. Marshall
Methodology: F. W. Goldsworth, H. L. Johnson, D. P. Marshall
Software: F. W. Goldsworth
Supervision: H. L. Johnson, D. P. Marshall
Visualization: F. W. Goldsworth
Writing – original draft: F. W. Goldsworth
Writing – review & editing: F. W. Goldsworth, H. L. Johnson, D. P. Marshall

Abstract Density staircases are observed in an idealized model of a deep western boundary current upon crossing the equator. We propose that the staircases are generated by the excitement of symmetric instability as the current crosses the equator. The latitude at which symmetric instability is excited can be predicted using simple scaling arguments. Symmetric instability generates overturning cells which, in turn, cause the inhomogenous mixing of waters with different densities. The mixing barriers and well mixed regions in density profiles coincide, respectively, with the boundaries and centers of the overturning cells generated by the symmetric instability. This new mechanism for producing density staircases may require us to re-evaluate the origins of some of the density staircases observed in the Tropical Atlantic.

Plain Language Summary In this study we demonstrate that waters of different density are mixed together in a deep western boundary current as it crosses the equator. We show that this is a result of the excitement of small-scale symmetric instabilities. The mixing generates density staircases which can affect the formation of dense waters and diapycnal mixing—processes which are important for maintaining the Atlantic Meridional Overturning Circulation. We use both a high-resolution computer model and a simple toy-model to explain how the staircases are generated. Historically, many density staircases have been observed in the region we are studying. We suggest that theories of how these staircases are generated may need revising given the findings of this study.

1. Introduction

The Atlantic Meridional Overturning Circulation (AMOC) is a global-scale system of currents that is important for transporting heat, salt and other tracers both laterally and vertically, including between hemispheres (Jackson et al., 2015). As such it plays an important role in the response of the climate system to anthropogenic forcing. There are two important cross-equatorial components to the AMOC—the northward-flowing surface-intensified North Brazil Current, and the southward-flowing Deep Western Boundary Current (Bower et al., 2019). At 5°S, the Deep Western Boundary Current transports 25.5 ± 8.3 Sv (1 Sv ≡ 10^6 m^3s^{-1}), at a depth between 1,200 m and 3,600 m below the surface, with a width of approximately 100 km and a peak velocity of around 20 cm s^{-1} (Schott et al., 2005). Goldsworth et al. (2021) showed that surface cross-equatorial western boundary currents may be susceptible to symmetric instability, but the susceptibility of deep western boundary currents to symmetric instability remains an open question. In this paper we show not only that deep western boundary currents are susceptible to symmetric instability, but that this instability can result in the formation of density staircases.

Density staircases are step-like features which can be seen in plots of seawater density against depth, and they are ubiquitous in the global ocean (Johannessen & Lee, 1974; Lambert & Sturges, 1977; Melling et al., 1984; Schmitt et al., 1987; Stern, 1960; Tait & Howe, 1968). The staircases consist of alternating well mixed regions with low stratification and thin interfaces with high stratification. The high stratification interfaces can form "mixing barriers" which inhibit the vertical transport of water properties such as heat and salt, whereas mixing is enhanced in the low stratification regions. Density staircases can affect both diapycnal mixing and water mass transformation rates (Schmitt et al., 2005), which are known to be important in closing the AMOC's overturning budget (de Lavergne et al., 2022). Many staircases are thought to form as a result of double diffusive convection, but other staircase generation mechanisms have been identified, such as inhomogeneous mixing (Balmforth et al., 1998). An example of a density staircase in the Deep Western Boundary Current, just south of the equator is explored in Text S1 in Supporting Information S1.

Symmetric instability is a type of submesoscale instability which occurs when the Ertel potential vorticity of a flow has the opposite sign to the planetary vorticity (Hoskins, 1974; Stone, 1966). The potential vorticity is defined as

$$Q = (\mathbf{f} + \nabla \times \mathbf{u}) \cdot \nabla b, \tag{1}$$

where $\mathbf{f}$ is the planetary vorticity vector, $\mathbf{u}$ is the velocity, and $b = -g\rho/\rho_0$ is the buoyancy. Potential vorticity with sign opposite to that of the vertical component of planetary vorticity, $\mathbf{k} \cdot \mathbf{f}$, is typically described as "anomalous." Anomalous potential vorticity can be generated through mechanical or diabatic forcing, or by changing the sign of planetary vorticity. In a deep western boundary current, to leading order, potential vorticity is conserved as the current is separated from the surface and bottom boundary layers in which mechanical and diabatic forcings can act. This means symmetric instability can only be induced via a change in sign of planetary vorticity, as occurs at the equator. Cross-equatorial symmetric instability is unique in this sense—it need not be confined to either the surface boundary layer or sloping bottom boundary layer (Haine & Marshall, 1998; Wenegrat & Thomas, 2020). A host of recent studies have identified regions where cross-equatorial symmetric instability may be excited (Forryan et al., 2021; Goldsworth et al., 2021; Jakoboski et al., 2022; Zhou et al., 2022).

In Section 2 we describe our idealized numerical model of a deep western boundary current crossing the equator. In Section 3 we demonstrate the formation of density staircases and the excitement of symmetric instability in the model, and propose that the staircases are generated as a result of the onset of symmetric instability. Simple scaling arguments are used to explain the differences between instabilities seen in deep western boundary currents and in surface intensified currents. Finally, in Section 4 we summarize our findings and explain the potential implications of these results.

2. Model Configuration

Simulations of an idealized deep western boundary current crossing the equator are performed using the MITgcm (Marshall et al., 1997). The domain size is 600 km in the zonal direction, 4,500 m in the vertical, and stretches from 2,000 km South to 1,000 km North in the meridional direction. The horizontal grid spacing is 1 km and the vertical grid spacing 10 m. The time-step is 144 s and the model is integrated for a total of 239 days. A second integration with a 2 km resolution and a 288 s time-step was performed and the findings presented below remained the same (see Text S2 in Supporting Information S1 for further detail). The model domain is sited on a β-plane. The meridional gradient in the vertical component of the Coriolis parameter is set to 2.3×10^{-11} s^{-1} m^{-1}, and the meridional component of the Coriolis parameter to 1.5×10^{-4} s^{-1}.

At the surface, a rigid lid boundary condition is employed. The lateral boundary conditions are set to be free-slip and the bottom boundary condition to no-slip. The sensitivity to the choice of boundary conditions was investigated by running a further integration with no-slip lateral and free-slip bottom boundary conditions. The findings presented below remained the same regardless of the boundary conditions used—see Text S2 in Supporting Information S1 for further details. The model has sloping bathymetry which can be seen in Figure 1b. The model is initialized by setting the meridional velocity and density profiles to those shown in Figure 1b, and with a zonal velocity of zero. The density profile is based on a neutral density (or γ^n) climatology aggregated from the area enclosed by the red rectangle in Figure 1a. The model is forced by prescribing the meridional velocity, zonal velocity, and the density, at the northern and southern domain boundaries. The same fields used to initialize the model are used as boundary conditions. A sponge region is placed at both the northern and southern edge of the domain. The northern sponge stretches from 900 to 1,000 km North and the southern sponge from 1,700 km to 2,000 km South. The inverse relaxation time-scale within the sponges varies from 1×10^{-5} s^{-1} (corresponding to a time scale of around 1.2 days) at the edge of the domain to 0 s^{-1} at the sponges' equatorward edges. The inverse relaxation time-scale takes the form of a hyperbolic tangent, with a characteristic length-scale of 5 km in the northern sponge and 10 km in the southern sponge.

A linear equation of state, is used, with a reference density of 1022.73 kg m^{-3} and thermal expansion coefficient of 2×10^{-4} K^{-1}. The linear equation of state avoids the complexities added by non-linear effects. The thermal diffusion coefficient is set to 1×10^{-5} m^2 s^{-1}. A second order-moment Prather advection scheme with a flux limiter is employed. Salinity is set to be constant and has no impact on the dynamics. Momentum dissipation is

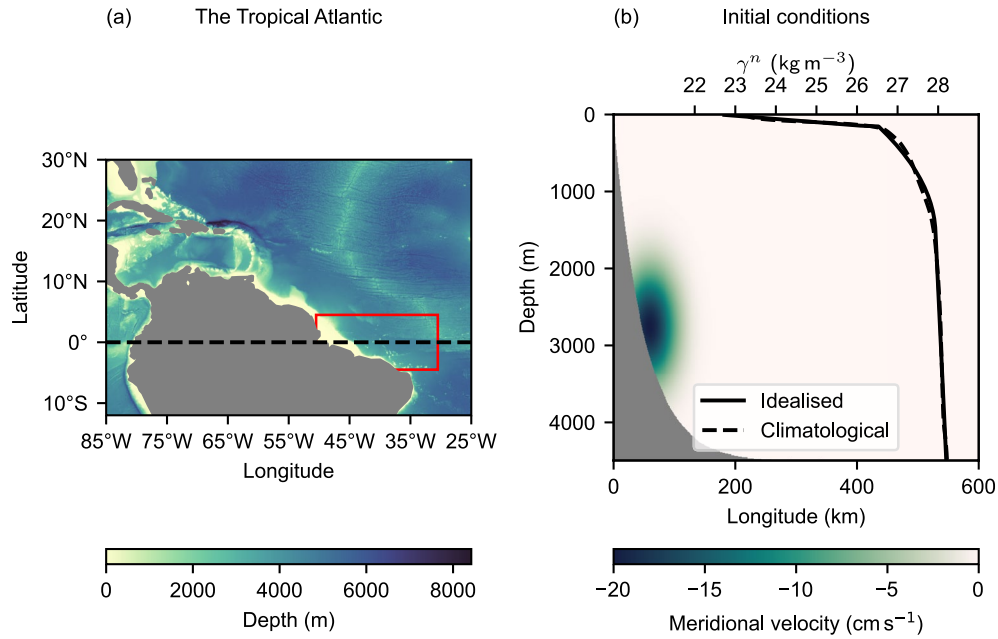

Figure 1. (a) Bathymetric map of the western tropical Atlantic. Climatological profiles of neutral density were aggregated from the area enclosed by the red rectangle. Bathymetry data from GEBCO Compilation Group (2020). (b) Meridional velocity profile (colors) and density profile (solid line) used as initial and boundary conditions for the model. The velocity profile is based on observations by Schott et al. (2005), and the density profile on the climatological mean (dashed line) (Boyer et al., 2018).

provided by a vertical Laplacian viscosity of 4×10^{-4} m^2 s^{-1} and an adaptive biharmonic Smagorinsky viscosity. Potential vorticity is calculated using the C-grid algorithm of Morel et al. (2019).

3. Symmetric Instability and Staircase Formation

Figure 2b shows $\partial_z b$ in the model after 239 days of integration 250 km south of the equator. Immediately apparent are the thin, sharp regions of high stratification (so called "mixing barriers") separating larger regions of well mixed waters with low and uniform stratification. Moving to 500 km south, we see in Figure 2c that some of the weaker barriers have dissipated; however the stronger barriers remain. Figure 2a shows the squared buoyancy frequency at the equator. At the outer edge of the current's core we see some weak mixing barriers.

Figure 3a shows the average of the meridional component of relative vorticity between 234 and 239 days of model integration in a region 250 km south of the equator. This can be thought of as a crude proxy for a zonal overturning streamfunction—it measures the local rotation around the meridional axis, that is, the amount of zonal overturning. We consider it here as the true zonal overturning streamfunction is ill-defined, since the flow is not invariant in the meridional direction. Examining the meridional vorticity, note that there are a series of counter-rotating stacked overturning cells between around 1,750 and 3,500 m below the surface. The black contours overlain show $\partial_z b = 2 \times 10^{-6}$ s^{-2} and help identify the locations of the mixing barriers in Figure 2b. We can see that the structure of the buoyancy frequency squared and the meridional vorticity are remarkably similar, with the horizontal edges of the overturning cells (vorticity zeros) approximately coinciding with the locations of the mixing barriers. This is also apparent in Figure 3b. The black line shows neutral density plotted as a function of depth at 250 km south and 90 km west (the location of the magenta lines and points shown in the other figures). The orange line shows the meridional component of relative vorticity at the same point. Both quantities have been averaged over the time period spanning 234–239 days. The treads of the steps in neutral density correspond to mixing barriers and the risers to well mixed regions. When comparing neutral density and the meridional vorticity we again see that the mixing barriers tend to coincide with vorticity zeros, whereas the mixing barriers coincide with vorticity extrema. This suggest that the inhomogeneous mixing driven by the overturning cells is what is causing the formation of the staircases.

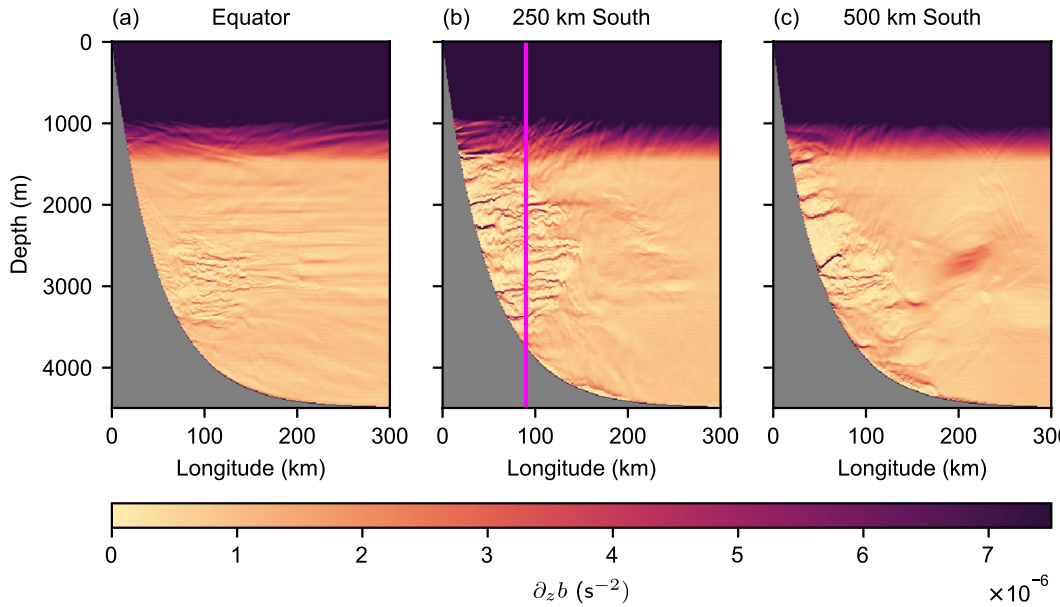

Figure 2. Squared buoyancy frequency after 239 days of model integration plotted at (a) the equator, (b) 250 km south of the equator, and (c) 500 km south of the equator. The figures show the presence of mixing barriers (thin filaments of strong stratification) separated by well mixed regions of low stratification. The magenta line indicates the location of the vorticity and density profiles shown in Figure 3. An animated version of this figure is shown in Movie S1 in Supporting Information S1.

3.1. A Very Simple Model of Staircase Formation

The differential mixing which produces the mixing barriers is analogous to the process which produces zonal jets on a β-plane (Manfroi & Young, 1999). Manfroi and Young (1999) study a sheared zonal flow on a β-plane and find that mixing in the presence of a meridional gradient in planetary vorticity leads to the preferential formation of zonal jets—high vorticity filaments. The meridional distance between the jets is set by the strength of the mixing. Here, instead of a meridional gradient in planetary vorticity there is a vertical gradient in buoyancy, and instead of mixing in the horizontal plane we have overturning in the vertical plane. This leads to the generation of high stratification filaments known as mixing barriers.

We can reproduce the formation of mixing barriers with a toy model, in which we consider how buoyancy changes over time as a result of vertical diffusion and advection by overturning cells. If we express the overturning motion as a streamfunction ψ where $u = -\partial_z \psi$ and $w = \partial_x \psi$ and use a constant harmonic diffusivity, κ we can express the evolution of b as

$$\frac{\partial b}{\partial t} = \frac{\partial \psi}{\partial z}\frac{\partial b}{\partial x} - \frac{\partial \psi}{\partial x}\frac{\partial b}{\partial z} + \kappa \frac{\partial^2 b}{\partial z^2}. \tag{2}$$

This is just the advection diffusion equation for a passive, conservative tracer being advected around the xz-plane. We choose $\psi = e^{-x^2/2\sigma^2} \sin(k_z z)$, to represent stacked overturning cells which are localized to a region of width σ in the horizontal. We also set $b\,(t = 0) = N^2 z$, and then solve the equation numerically using a third order Adam's Bashforth scheme on a domain stretching from −50 to 50 km in the horizontal and spanning 600 m in the vertical. We set $\sigma = 25$ km, $k_z = 2\pi/200$ m^{-1}, $\kappa = 1 \times 10^{-5}$ m^2 s^{-1} and $N^2 = 1 \times 10^{-6}$ s^{-2}. The grid spacing is set to 1 km in the horizontal and 2.5 m in the vertical, and the time step is 240 s. Gravitational instability is parameterized by setting κ to an enhanced value of 5×10^{-3} m^2 s^{-1} in regions where $\partial_z b \leq 0$.

The stratification is shown at three different times in Figures 3c–3e. Alternating high and low stratification regions develop with time. Initially this is a result of differential mixing; however, at later times the mixing barriers become sharper and start to form filaments due to gravitational instability in the low stratification regions producing extra mixing. In the ocean, it is likely that other secondary instabilities will be excited before the flow

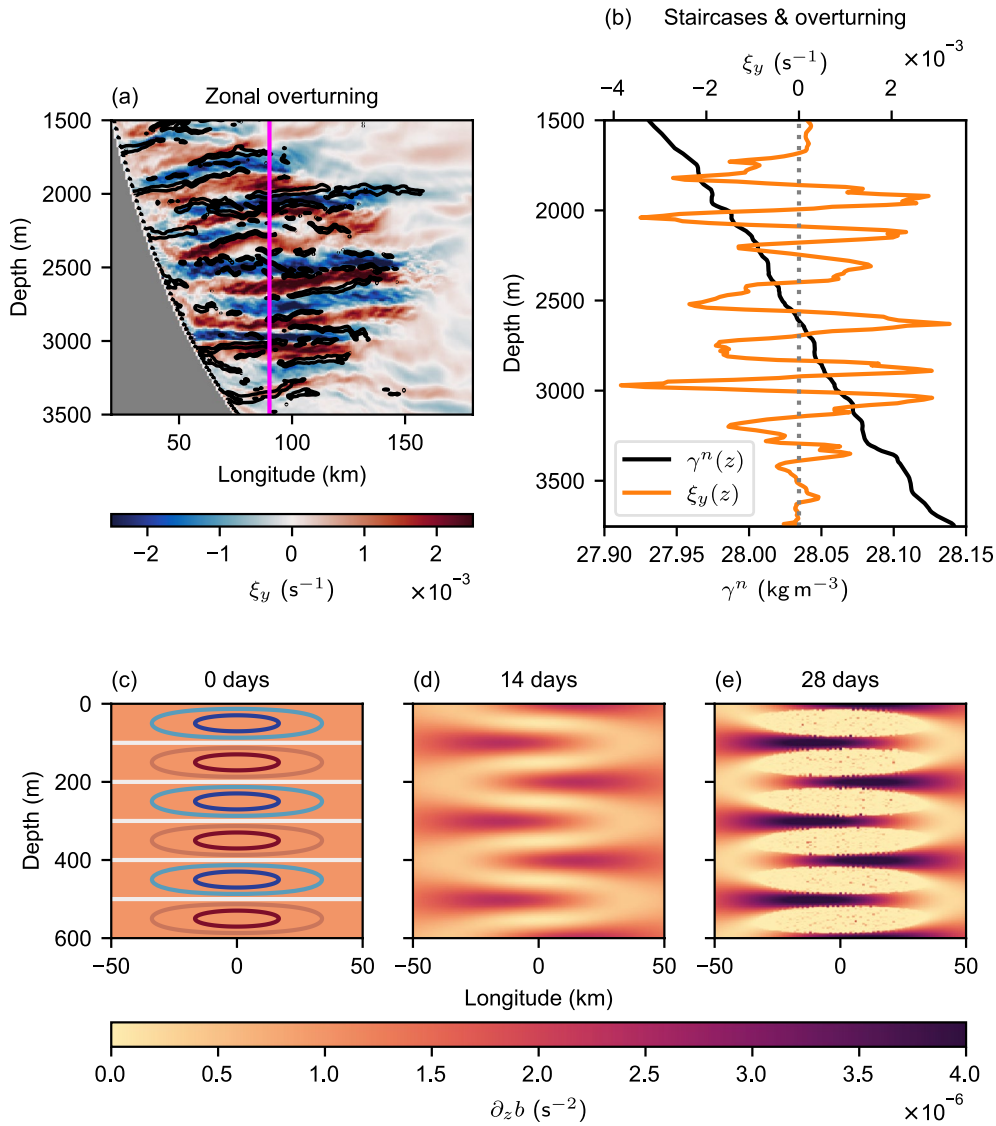

Figure 3. (a) Time mean meridional component of relative vorticity between 234 and 239 days of model integration, plotted as a function of longitude and depth, at 250 km south. Alternating red and blue cells indicate the presence of stacked zonal overturning cells. Overlain is the contour defined by $\partial_z b = 2 \times 10^{-6}$ s^{-2}, indicating the locations of the mixing barriers. (b) Density (black line) and time mean meridional component of relative vorticity (orange line) plotted as a function of depth at 90 km west and 250 km south (shown on other figures as a magenta line or point). Vorticity extrema coincide with well mixed regions and zeros with mixing barriers suggesting the density staircases are formed by the overturning cells. Panels (c–e) show snapshots of the stratification over time from the toy model, showing how the mixing barriers begin to form in the presence of inhomogeneous mixing. The contours on panel (c) show the overturning streamfunction. An animated version of the lower panels of this figure are shown in Movie S2 in Supporting Information S1.

becomes gravitationally unstable; however, the simple model uses fixed circulations, so in this set up gravitational instability produces the extra mixing (via a parameterization).

3.2. But What Is Generating the Overturning?

Previous work by Goldsworth et al. (2021) has demonstrated that western boundary currents can become unstable when crossing the equator as they advect anomalous potential vorticity from one hemisphere into the other. In Figure 4a, which shows the potential vorticity on the $\gamma^n = 28.04$ surface, we can see the advection of positive potential vorticity from the northern hemisphere into the southern hemisphere, so we may expect to see symmetric instability excited south of the equator. The excitement of the instability is apparent in a region from around

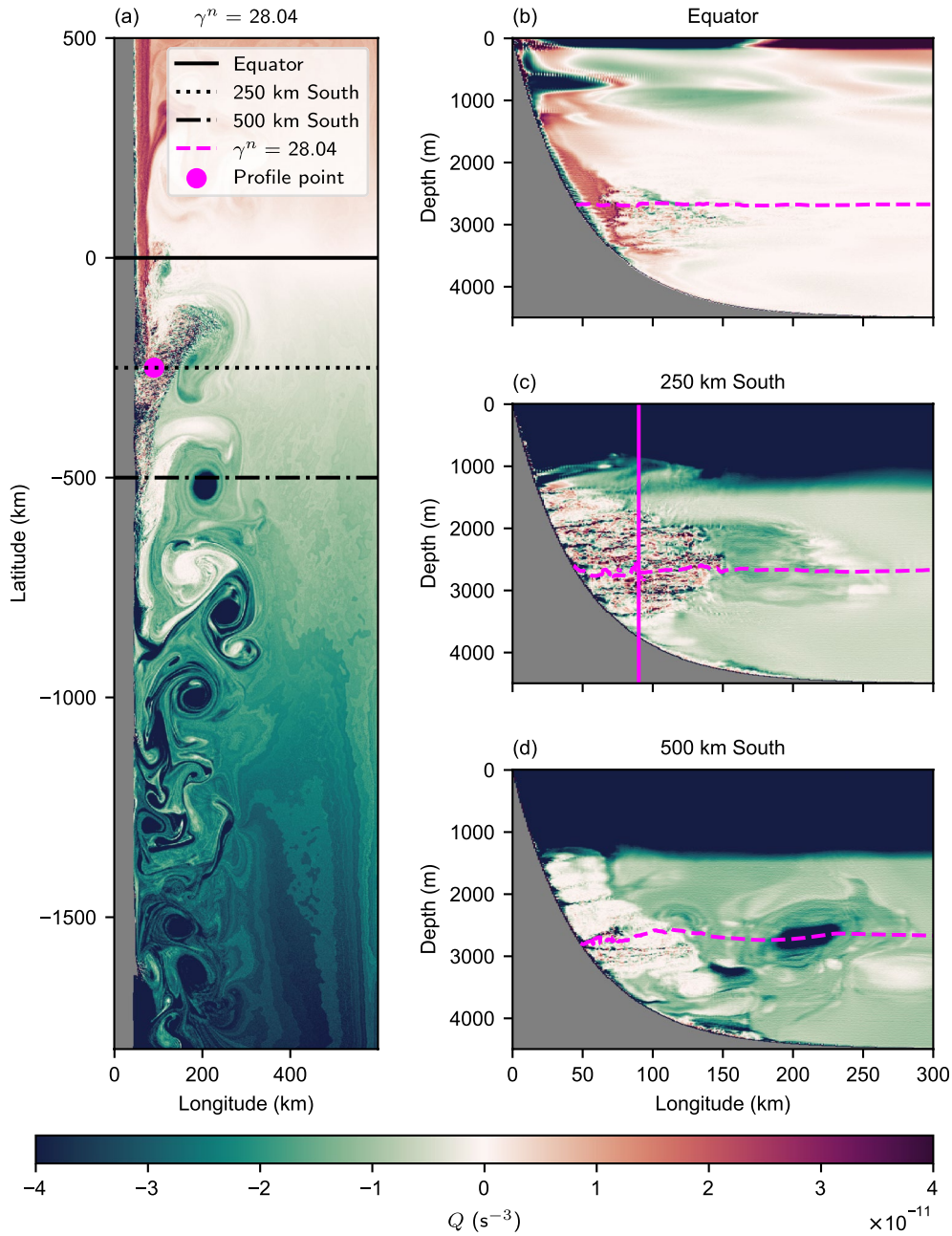

Figure 4. Potential vorticity after 239 days of model integration plotted on (a) the $\gamma^n = 28.04$ surface, (b) at the equator, (c) at 250 km south of the equator, and (d) at 500 km south of the equator. Black lines show the latitudes at which sections have been plotted. The figures show the advection of positive potential vorticity from the northern hemisphere into the southern hemisphere and the excitement of symmetric instability. The solid magenta line and point indicate the location of the vorticity and density profiles shown in Figure 3. The dashed magenta line shows the $\gamma^n = 28.04$ surface. An animated version of this figure is shown in Movie S3 in Supporting Information S1.

25–600 km south of the equator. Figures 4b–4d show the potential vorticity as a function of depth and longitude at, the equator, 250 km south and 500 km south respectively, after 239 days of model integration. At the equator we see the advection of waters with positive potential vorticity into the southern hemisphere. At 250 km south we can see the excitement of symmetric instability, and by 500 km south we can see large pools of neutral potential vorticity suggesting the waters here have experienced symmetric instability, with the excitement of symmetric instability still underway at around 3,000 m. In Figure 4b we also see symmetric instability like patterns in a region of negative potential vorticity. Movie S3 in Supporting Information S1 shows that this is the result of the

retroflection of symmetrically unstable waters crossing the equator from south to north. This also explains the presence of the weak staircases at the equator seen in Figure 2a.

The vertical spacing between the overturning cells and mixing barriers seen in the numerical model is approximately 120 m. This suggests that when searching for evidence of symmetric instability in observations of the Deep Western Boundary Current we should look for mixing barrier spacings of this width. However, it has been shown that the vertical length-scale of the overturning cells generated by symmetric instability are controlled by the stratification and the rate of dissipation within the fluid (Goldsworth et al., 2021; Griffiths, 2003; Plougonven & Zeitlin, 2009). In our model, we represent dissipation as an eddy viscosity, which is several orders of magnitude higher than the molecular viscosity of sea-water—this viscosity represents unresolved mixing processes within our model. In reality it will be neither the model's eddy viscosity nor sea-water's molecular viscosity that sets the length-scale of the overturning cells. Kelvin-Helmholtz instabilities, rather than molecular diffusion are known to be the predominant dissipation mechanism for the overturning cells generated by symmetric instabilities (Griffiths, 2003; Taylor & Ferrari, 2009). Based on the work of others, we estimate a model resolution of 25 m would be required to adequately resolve such processes, which would require approximately 10^4 times more computational resources than those used in the numerical model considered here, making such calculations unfeasible (Taylor & Ferrari, 2009; Yankovsky & Legg, 2019).

In the limit of no vertical shear it is possible to obtain an analytic estimate of the overturning cell spacing, for a given velocity profile, latitude, stratification and viscosity. For the Deep Western Boundary Current, all of these parameters are either known or observationally constrained, with the exception of viscosity which sets the rate of dissipation. As previously discussed, we know that the value must be greater than the molecular viscosity of sea-water, but lower than a typical eddy viscosity used in numerical models. We can use this to put a lower and an upper limit on the size of the staircases we expect to see in the ocean.

For a flow symmetric in the y direction we expect the overturning streamfunction generated by symmetrically unstable motions to be expressed as $\psi(x,z,t) = \hat{\psi}(x)e^{i(k_z z - \omega t)}$. Plougonven and Zeitlin (2009) show that on an f-plane in the limit of no vertical shear, this streamfunction satisfies the equation

$$\frac{\left(\hat{\omega}^2 - N^2\right)}{k_z^2}\frac{\mathrm{d}^2\hat{\psi}}{\mathrm{d}x^2} + f\zeta\hat{\psi} = \hat{\omega}^2\hat{\psi}, \tag{3}$$

where $\hat{\omega} = \omega + i\kappa k_z^2$, ζ is the absolute vorticity of the flow, and f is the vertical component of the Coriolis parameter. In the above we see that overturning cells with a whole spectrum of vertical wavenumbers are generated by the action of symmetric instability. However, stratification suppresses the growth of cells with low wavenumbers, whereas dissipation suppresses the growth of cells with large wavenumbers—this means that there exists an overturning cell with a vertical wavenumber which maximizes its growth rate, and that this cell will become the dominant mode within a few e-folding timescales. Solving the eigenvalue problem for fixed values of f, N^2, ζ and κ, we can find the value of k_z which maximizes the imaginary component of ω, that is, the overturning cell with the largest growth rate.

As before, we set $N^2 = 1 \times 10^{-6}\ \mathrm{s}^{-2}$. We use the Bickley jet as a model of the velocity field, that is,

$$V(x) = V_0\left(1 - \tanh^2\left(\frac{x - x_{mid}}{\delta_b}\right)\right) \tag{4}$$

with $V_0 = -0.2\ \mathrm{m\,s}^{-1}$, $x_{mid} = 60$ km and $\delta_b = 30$ km. We set $f = -1.91 \times 10^{-6}\mathrm{s}^{-1}$ which corresponds to a latitude of 0.75°S and κ to either $1 \times 10^{-6}\ \mathrm{m^2\,s^{-1}}$ or $4 \times 10^{-4}\ \mathrm{m^2\,s^{-1}}$, representing the viscosity of seawater and a typical eddy viscosity, respectively. The step size of the staircase is half the vertical wavelength of the overturning cells, giving step sizes of between 13 and 90 m. This constrains the size of the staircases produced by symmetric instability in the Deep Western Boundary Current to within an order of magnitude. To confirm whether an observed staircase has been formed by the action of symmetric instability or some other process will require supplementary observations. If the absolute vorticity (or better still, potential vorticity) of the flow is near-zero, it is likely a staircase will have been formed by symmetric instability (Castelão & Johns, 2011; Goldsworth et al., 2021). Strong lateral coherence within around 100 km of the boundary would also be indicative of a staircase formed by the action of symmetric instability in the Deep Western Boundary Current—seismic imaging techniques may be particularly effective for identifying such features (Fer et al., 2010). If a staircase has variable step size, in the event it has

been formed by symmetric instability, we would expect to see larger steps where the background stratification is weaker and smaller steps where the background stratification is stronger.

3.3. Estimating at Which Latitudes Symmetric Instability Occurs

Unlike in the study of Goldsworth et al. (2021), we see the excitement of symmetric instability close to the equator followed by the formation of eddies, whereas in the former study we see the spinning up of large anti-cyclonic eddies followed by the excitement of symmetric instability further away from the equator. This is due to the reduced growth rate of barotropic instability in the deep western boundary current (Edwards & Pedlosky, 1998), meaning that symmetric instability dominates over short time-scales. This is further exacerbated by the anti-cyclonic eddies seen by Goldsworth et al. (2021), which act to reduce the growth rate of the symmetric instability in their experiments, allowing anomalous potential vorticity to persist whilst the eddies grow (Buckingham et al., 2021).

We can in fact be more quantitative about the latitude at which the instability is forming. There is an e-folding timescale, τ_e, associated with symmetric instability which can be converted into an advective meridional length scale, y with the equation $y = V\tau_e$, where V is a typical meridional velocity. From linear stability theory we know that for a parallel shear flow, like a deep western boundary current (Hoskins, 1974) the time scale of symmetric instability is given by

$$\tau_e \sim \left(\beta y\left(f + \frac{V}{L_x}\right)\right)^{-1/2} \tag{5}$$

and that for the case of an eddy, such as a North Brazil Current ring, the symmetric instability timescale is (Buckingham et al., 2021)

$$\tau_e \sim \left(\beta y\left(f + \frac{2V}{R}\right)\right)^{-1/2}. \tag{6}$$

We can then convert these expressions to a meridional length scale, giving

$$y \sim \sqrt[3]{\frac{VL_x}{\beta}} \tag{7}$$

for parallel shear flows, and for an eddy

$$y \sim \sqrt[3]{\frac{2VR}{\beta}}. \tag{8}$$

In the case of the eddying flow, we have assumed the meridional velocity is of a similar order of magnitude to the azimuthal velocity. In both expressions we have assumed y to be small and only considered terms of the lowest order in y. We can now evaluate the expressions for the latitude of the onset of symmetric instability. For the deep western boundary current we choose $V \sim 0.2$ m s^{-1}, $L_x \sim 30$ km and $\beta \sim 2.3 \times 10^{-11}$ m^{-1} s^{-1}, giving $y \sim 60$ km. For the North Brazil Current rings we choose $V \sim 1$ m s^{-1}, $R \sim 100$ km and the same value for β, giving $y \sim 200$ km. These predictions of the latitude of instability are of the same order of magnitude as those we see in the numerical models. In the case of North Brazil Current rings, Goldsworth et al. (2021) see instability at around 400 km north, and in this study we see instability from around 25 km north of the equator.

4. Conclusions

Density staircases are step-like features which become apparent when density is plotted as a function of depth and are common throughout the Earth's oceans. In an idealized model of a deep western boundary current crossing the equator we see density staircases form. The staircases are generated by overturning cells which are in turn generated by the excitement of symmetric instability as the current crosses the equator. Symmetric instability in cross-equatorial flows is excited due to the advection of anomalous potential vorticity from one hemisphere to another. The stacked overturning cells that generate the staircases are, however, a feature of symmetric instability regardless of what is forcing it, suggesting we may see staircase formation in other symmetrically unstable flows, including when anomalous potential vorticity is induced by frictional torques or diabatic processes. Differences

in the latitude of instability between surface intensified western boundary currents and deep western boundary currents can be adequately explained using simple scaling arguments relating to growth rates of symmetric instability and advective timescales.

It is thought that diapycnal mixing may play an important role in closing the overturning budget of the Atlantic Meridional Overturning Circulation's deep limb. Figures 2 and 4 clearly show that vigorous mixing is taking place; however, accurately calculating the amount of mixing that is occurring is tricky. This is due to the importance of secondary Kelvin Helmholtz instabilities in transforming water masses. In order to resolve these processes we would need a model with around 40 times the resolution used here (e.g., Yankovsky and Legg, 2019), which is computationally infeasible—such a model would require at least 10^4 times more computational resources to run. Simplified two dimensional models may help in accurately quantifying the induced diapycnal mixing, however. It is not clear whether such processes would enhance or erode the staircases we observe here. We hypothesize that the instability will be most active in regions of large shear which corresponds to the well mixed regions at the overturning cell centers. This would lead to an enhancement of the staircases; however, only further experiments can confirm this. Furthermore, we hypothesize that weaker staircases will be eroded more quickly by isotropic turbulence.

Density staircases are well documented in the Tropical Atlantic and are often said to form as a result of salt fingering and double diffusive convection (e.g., Schmitt et al., 1987; Schmitt et al., 2005). In light of this work, we suggest new insights into mixing in the region could be gained by revisiting existing observations and reexamining the origins of observed staircases. Using linear stability theory, we estimate that the step-size of staircases generated by symmetric instability in the Deep Western Boundary Current will be in the range 13–90 m. They will be accompanied by waters with near zero potential vorticity, have strong lateral coherence and the step-size will vary with stratification.

Data Availability Statement

Model integrations were run using the MITgcm model (checkpoint 68i) (Campin et al., 2022) on the ARCHER2 HPC facility. The git repository Goldsworth et al. (2022b) contains model configuration files, and the python scripts used for analyzing the model output. The repository Goldsworth et al. (2022a) contains the data required to recreate the model's initial conditions and a subset of processed model output. The analysis performed on the data made heavy use of the open source xarray (Hoyer & Hamman, 2017), xmitgcm (Abernathey et al., 2021) and Dask (Dask Development Team, 2016) software libraries.

Acknowledgments
We are grateful for the financial support of the Natural Environment Research Council NE/L002612/1. This work used the ARCHER2 UK National Supercomputing Service (https://www.archer2.ac.uk). We would also like to thank two anonymous reviewers for their helpful comments which improved this manuscript.

References

Abernathey, R., Dussin, R., Smith, T., Fenty, I., Bourgault, P., Jones, S., et al. (2021). MITgcm/xmitgcm: v0.5.2 (Version v0.5.2) [Computer Software]. Zenodo. https://doi.org/10.5281/ZENODO.5139886

Balmforth, N. J., Llewellyn Smith, S. G., & Young, W. R. (1998). Dynamics of interfaces and layers in a stratified turbulent fluid. *Journal of Fluid Mechanics*, *355*, 329–358. https://doi.org/10.1017/S0022112097007970

Bower, A., Lozier, S., Biastoch, A., Drouin, K., Foukal, N., Furey, H., et al. (2019). Lagrangian views of the pathways of the Atlantic Meridional Overturning Circulation. *Journal of Geophysical Research: Oceans*, *124*(8), 5313–5335. https://doi.org/10.1029/2019JC015014

Boyer, T. P., Garcia, H. E., Locarnini, R. A., Zweng, M. M., Mishonov, A. V., Reagan, J. R., et al. (2018). World Ocean Atlas 2018. *Temperature and salinity*. Retrieved from https://www.ncei.noaa.gov/archive/accession/NCEI-WOA18

Buckingham, C. E., Gula, J., & Carton, X. (2021). The role of curvature in modifying frontal instabilities. Part I: Review of theory and presentation of a nondimensional instability criterion. *Journal of Physical Oceanography*, *51*(2), 299–315. https://doi.org/10.1175/JPO-D-19-0265.1

Campin, J.-M., Heimbach, P., Losch, M., Forget, G., Edhill3, Adcroft, A., et al. (2022). MITgcm/MITgcm: checkpoint68i (Version checkpoint68i) [Computer Software]. Zenodo. https://doi.org/10.5281/ZENODO.6498956

Castelão, G. P., & Johns, W. E. (2011). Sea surface structure of North Brazil Current rings derived from shipboard and moored acoustic Doppler current profiler observations. *Journal of Geophysical Research*, *116*(1), C01010. https://doi.org/10.1029/2010JC006575

Dask Development Team. (2016). Dask: Library for dynamic task scheduling. [Computer software manual]. Retrieved from https://dask.org

de Lavergne, C., Groeskamp, S., Zika, J., & Johnson, H. L. (2022). Chapter 3 - The role of mixing in the large-scale ocean circulation. In M. Meredith & A. Naveira Garabato (Eds.), *Ocean mixing* (pp. 35–63). Elsevier. https://doi.org/10.1016/B978-0-12-821512-8.00010-4

Edwards, C. A., & Pedlosky, J. (1998). Dynamics of nonlinear cross-equatorial flow. Part II: The tropically enhanced instability of the western boundary current. *Journal of Physical Oceanography*, *28*(12), 2407–2417. https://doi.org/10.1175/1520-0485(1998)028⟨2407:DONCEF⟩2.0.CO;2

Fer, I., Nandi, P., Holbrook, W. S., Schmitt, R. W., & Páramo, P. (2010). Seismic imaging of a thermohaline staircase in the western tropical North Atlantic. *Ocean Science*, *6*(3), 621–631. https://doi.org/10.5194/os-6-621-2010

Forryan, A., Naveira Garabato, A. C., Vic, C., Nurser, A. J., & Hearn, A. R. (2021). Galápagos upwelling driven by localized wind–front interactions. *Scientific Reports*, *11*(1), 1–12. https://doi.org/10.1038/s41598-020-80609-2

GEBCO Compilation Group. (2020). Gebco 2020 grid [Dataset]. https://doi.org/10.5285/a29c5465-b138-234d-e053-6c86abc040b9

Goldsworth, F. W., Johnson, H. L., & Marshall, D. P. (2022a). Data for "Density staircases generated by symmetric instability in a cross-equatorial deep western boundary current". [Dataset]. https://doi.org/10.5281/zenodo.7304012

Goldsworth, F. W., Johnson, H. L., & Marshall, D. P. (2022b). dwbc-proj [Software]. Retrieved from https://www.github.com/fraserwg/dwbc-proj/tree/v1.2. https://doi.org/10.5281/zenodo.7304353

Goldsworth, F. W., Marshall, D. P., & Johnson, H. L. (2021). Symmetric instability in cross-equatorial western boundary currents. *Journal of Physical Oceanography*, *1*(6), 2049–2067. https://doi.org/10.1175/JPO-D-20-0273.1

Griffiths, S. D. (2003). Nonlinear vertical scale selection in equatorial inertial instability. *Journal of the Atmospheric Sciences*, *60*(7), 977–990. https://doi.org/10.1175/1520-0469(2003)060⟨0977:NVSSIE⟩2.0.CO;2

Haine, T. W. N., & Marshall, J. (1998). Gravitational, symmetric, and baroclinic instability of the ocean mixed layer. *Journal of Physical Oceanography*, *28*(4), 634–658. https://doi.org/10.1175/1520-0485(1998)028⟨0634:gsabio⟩2.0.co;2

Hoskins, B. J. (1974). The role of potential vorticity in symmetric stability and instability. *Quarterly Journal of the Royal Meteorological Society*, *100*(425), 480–482. https://doi.org/10.1002/qj.49710042520

Hoyer, S., & Hamman, J. (2017). xarray: N-D labeled arrays and datasets in Python. *Journal of Open Research Software*, *5*(1), 10. https://doi.org/10.5334/jors.148

Jackson, L. C., Kahana, R., Graham, T., Ringer, M. A., Woollings, T., Mecking, J. V., & Wood, R. A. (2015). Global and European climate impacts of a slowdown of the AMOC in a high resolution GCM. *Climate Dynamics*, *45*(11–12), 3299–3316. https://doi.org/10.1007/s00382-015-2540-2

Jakoboski, J., Todd, R. E., Owens, W. B., Karnauskas, K. B., & Rudnick, D. L. (2022). Potential vorticity and instability in the Pacific equatorial undercurrent west of the Galápagos Archipelago. *Journal of Physical Oceanography*, *52*(8), 1927–1943. https://doi.org/10.1175/JPO-D-21-0124.1

Johannessen, O. M., & Lee, O. S. (1974). A deep stepped thermo-haline structure in the Mediterranean. *Deep-Sea Research and Oceanographic Abstracts*, *21*(8), 629–639. https://doi.org/10.1016/0011-7471(74)90047-3

Lambert, R. B., & Sturges, W. (1977). A thermohaline staircase and vertical mixing in the thermocline. *Deep-Sea Research*, *24*(3), 211–222. https://doi.org/10.1016/S0146-6291(77)80001-5

Manfroi, A. J., & Young, W. R. (1999). Slow evolution of zonal jets on the beta plane. *Journal of the Atmospheric Sciences*, *56*(5), 784–800. https://doi.org/10.1175/1520-0469(1999)056⟨0784:SEOZJO⟩2.0.CO;2

Marshall, J., Adcroft, A., Hill, C., Perelman, L., & Heisey, C. (1997). A finite-volume, incompressible Navier stokes model for, studies of the ocean on parallel computers. *Journal of Geophysical Research C: Oceans*, *102*(C3), 5753–5766. https://doi.org/10.1029/96JC02775

Melling, H., Lake, R., Topham, D., & Fissel, D. (1984). Oceanic thermal structure in the Western Canadian Arctic. *Continental Shelf Research*, *3*(3), 233–258. https://doi.org/10.1016/0278-4343(84)90010-4

Morel, Y., Gula, J., & Ponte, A. (2019). Potential vorticity diagnostics based on balances between volume integral and boundary conditions. *Ocean Modelling*, *138*(April), 23–35. https://doi.org/10.1016/j.ocemod.2019.04.004

Plougonven, R., & Zeitlin, V. (2009). Nonlinear development of inertial instability in a barotropic shear. *Physics of Fluids*, *21*(10), 106601. https://doi.org/10.1063/1.3242283

Schmitt, R. W., Ledwell, J. R., Montgomery, E. T., Polzin, K. L., & Toole, J. M. (2005). Ocean science: Enhanced diapycnal mixing by salt fingers in the thermocline of the tropical Atlantic. *Science*, *308*(5722), 685–688. https://doi.org/10.1126/science.1108678

Schmitt, R. W., Perkins, H., Boyd, J. D., & Stalcup, M. C. (1987). C-SALT: An investigation of the thermohaline staircase in the western tropical North Atlantic. *Deep-Sea Research, Part A: Oceanographic Research Papers*, *34*(10), 1655–1665. https://doi.org/10.1016/0198-0149(87)90014-8

Schott, F. A., Dengler, M., Zantopp, R., Stramma, L., Fischer, J., & Brandt, P. (2005). The shallow and deep western boundary circulation of the South Atlantic at 5°-11°S. *Journal of Physical Oceanography*, *35*(11), 2031–2053. https://doi.org/10.1175/JPO2813.1

Stern, M. E. (1960). The "salt-fountain" and thermohaline convection. *Tellus*, *12*(2), 172–175. https://doi.org/10.3402/tellusa.v12i2.9378

Stone, P. H. (1966). On non-geostrophic baroclinic stability. *Journal of the Atmospheric Sciences*, *23*(4), 390–400. https://doi.org/10.1175/1520-0469(1966)023⟨0390:ONGBS⟩2.0.CO;2

Tait, R., & Howe, M. (1968). Some observations of thermohaline stratification in the deep ocean. *Deep-Sea Research and Oceanographic Abstracts*, *15*(3), 275–280. https://doi.org/10.1016/0011-7471(68)90005-3

Taylor, J. R., & Ferrari, R. (2009). On the equilibration of a symmetrically unstable front via a secondary shear instability. *Journal of Fluid Mechanics*, *622*, 103–113. https://doi.org/10.1017/S0022112008005272

Wenegrat, J. O., & Thomas, L. N. (2020). Centrifugal and symmetric instability during Ekman adjustment of the bottom boundary layer. *Journal of Physical Oceanography*, *50*(6), 1793–1812. https://doi.org/10.1175/JPO-D-20-0027.1

Yankovsky, E., & Legg, S. (2019). Symmetric and baroclinic instability in dense shelf overflows. *Journal of Physical Oceanography*, *49*(1), 39–61. https://doi.org/10.1175/JPO-D-18-0072.1

Zhou, H., Dewar, W., Yang, W., Liu, H., Chen, X., Li, R., et al. (2022). Observations and modeling of symmetric instability in the ocean interior in the Northwestern Equatorial Pacific. *Communications Earth & Environment*, *3*(1), 28. https://doi.org/10.1038/s43247-022-00362-4

References From the Supporting Information

Atwood, D. K. (2022). CTD data from cruise 3175MB91, CF netCDF version [Dataset]. Retrieved from https://cchdo.ucsd.edu/cruise/3175MB91